공학석사 학위논문

Magenetic Nanoparticle Embedded Hydrogel Sheet with Groove Pattern for Wound Healing

자성나노입자와 그루브패턴 임베디드 하이드로젤 기반 시트제작을 통한 피부재생유도

2018. 08

서울대학교 대학원

협동과정 바이오엔지니어링 전공

노미연

Abstract

Magnetic Nanoparticle Embedded Hydrogel Sheet with Groove Pattern for Wound Healing

Miyeon Noh
Interdisciplinary Program in Bioengineering
The Graduate School
Seoul National University

Endothelial progenitor cell (EPC) is endothelial precursor cell that secretes bioactive factors to induce angiogenesis and vascularization. Due to its property, transplantation of EPC is one of ideal methods for wound therapy. Maximizing healing efficacy of EPC by maintaining cell retention and function, highly efficient scaffold is required for local delivery. Herein, we fabricated magnetic nanoparticle(MNP) embedded hydrogel sheet with groove pattern to promote vascularization for wound healing. We demonstrated that topographical modification of the surface with groove pattern induced cell proliferation, cell alignment and cell elongation. In addition, stimulation with patterned substrate prompted morphological changes mimicking endothelial stalk cell and tip cell like with branching

points, which consequently increased cell-cell interaction and secretion of growth factors such as PDGF-BB. As a result, enhanced wound healing was observed with efficient delivery of the MNP embedded patterned sheet (MPS) without deformation through magnetic force.

In this paper, enhancement of vascularization and repair of dermal wound with EPC/MPS will be reported.

Keywords: Groove pattern, magnetic nanoparticle, hydrogel, wound healing, vascularization, angiogenesis

Student Number : 2016-27768

CONTENTS

ABSTRACT 1
CONTENTS 3
LISTS OF FIGURES AND TABLES 4

CHAPTER 1. SCIENTIFIC BACKGROUND 5
1.1 Skin tissue engineering with Hydrogel 5
1.2 Endothelial Progenitor Cells in wound healing 6
1.3 cell alignment and cell elogation 7
1.4 Topographical surface modification 8

CHAPTER 2. MNP embedded hydrogel sheet with groove pattern fabrication and their commitment on wound healing 10
2.1 Introduction 10
2.2 Materials and methods 11
2.3 Results 19
2.4 Discussion 43

CONCLUSION 47

REFERENCE 48

요약(국민초록) 52

LISTS OF FIGURES AND TABLES

Figure 1. Scheme for synthesis of MNP embedded hydrogel sheet with groove pattern for wound healing.....26

Figure 2. Characterization of MNP embedded sheet 27

Figure 3. Characterization of Layer-by-Layered coated sheet 28

Figure 4. Characterization of hydrogel sheets with various groove patterns 29

Figure 5. Characterization of cell morphology 30

Figure 6. Cell viablity test on sheets.....31

Figure 7. Cell adhesion test on sheets 32

Figure 8. Cell proliferation assay.....33

Figure 9. Endothelial differentiation of endothelial progenitor cells 34

Figure 10. Cumulative release of cytokine from EPCs.....35

Figure 11. *In vitro* wound healing assay 36

Figure 12. *In vivo* wound healing 37

Figure 13. Vessel formation 38

Figure 14. Histological analysis of H&E 7days after surgery.....39

Figure 15. Histological analysis of H&E 14days after surgery 40

Figure 16. Immunohistochemistry of CD31 7days after surgery.....41

Figure 17. Immunohistochemistry of α-SMA 7days after surgery.....42

CHAPTER 1.

1.1 Skin tissue engineering with Hydrogel

Skin regeneration following infliction of large wound is important procedure in that skin is an outer barrier to protect not only organs from detrimental pathogen but also penetration of external environment elements such as UV [1]. To accelerate the repair of dermal wound and reduce the size of scar, development of wound dressing materials and attempts to deliver bioactive therapeutic growth factors and cells have been widely carried out[2]. However, challenges still lie in inducing rapid wound repair, considering poor growth factor/cell retention and stability to maintain their function. In this aspect, synthesis of appropriate carriers of target materials to enhance healing effect is needed.

Hydrogel has substantial potential as a carrier of cells, drug, and bioactive molecules such as growth factors for tissue regeneration. Especially, hydrogel can be used to mimic the physical and biochemical properties of extracellular matrices (ECM) with various engineering methods [3]. Given its suitable characteristic, many researchers have been studying development of materials for tissue repair with hydrogel. Therefore, hydrogel is also one of ideal materials for the skin tissue regeneration through fabrication of hydrogel based-scaffold to attach and culture the cells.

With regard to designing an effective scaffold to deliver the cells, biocompatibility, biodegradability, implant-ability, and high affinity with therapeutic factors by substrate modification must be considered.

1.2 Endothelial Progenitor Cells in wound healing

Endothelial progenitor cell (EPC) is defined as a stem cell which has potential to differentiate to endothelial cells that induce vascular regeneration and vessel formation. Neovascularization is essential for recovery of diverse disease as well as vascular injury implying that supply of oxygen and nutrients through blood circulating system plays an important role in helping repair of damaged tissue. EPC is encouraging resource as a therapeutic option for re-vascularization considering its secretion of various cytokines such as VEGF, PDGF-BB, SDF-1, IGF-1 and HGF. These growth factors contribute to differentiation of EPC to endothelial cells, activation of the resident mature endothelial cells, cell proliferation and migration [4-9]. Therefore, EPCs are widely used to enhance angiogenesis and vascularization, for treatment of vascular tissue regeneration.

Due to their ability to release various cytokines and prompt re-epithelialization, EPCs have been also used to treat wound healing [10-13]. There are 4 phases of wound healing; hemostasis, inflammatory, proliferative and remodeling and all of these phases are influenced with blood mediated-bioactive molecules. PDGF-BB is platelet derived growth factor with recombinant b chain homodimers and accelerates tissue repair

through inflammatory and proliferative phases. It stimulates sequential migration of neutrophils, macrophage and fibroblast to the wound area, yield of other growth factors such as VEGF, and promotes collagen synthesis, cell proliferation, and vascularization [14].

1.3 Cell alignment and cell elongation

Endothelial cells reside in the environment exposed to mechanical stimulation by blood flow. From the effect of shear stress, the cells change their morphology as compared to the state without the stimuli. The cells which initially have cobble stone like morphology align perpendicular to the strain and elongate their length. When they form aligned and elongated morphology, the cellular function is also influenced. Some research groups verified that stimulation by the physical modification of the cell surrounding environment triggers activation of intercellular signal and cytoskeletal changes [14-16]. Further, inducing endothelial cell alignment and elongation like native tissue increases cell-cell interaction, cell proliferation and migration [17].

Through the alteration of the cell structure, generation of new vasculature emerges, which is organized with three cell types; tip cell, stalk cell and phalanx cell. Tip cells leading the growing vascular sprouts are followed by stalk cells which proliferate and extend the vessel. Tip cells make larger their branches and motivate cell migration to establish vascular network [18, 19]. In addition, PDGF-BB is secreted from these tip cells and

prompts maturation of vascularization [20]. Therefore, endothelial cell alignment and elongation plays an important role in repairing wound.

1.4 Topographical surface modification

To induce cell alignment and maturation of endothelial cell through cell elongation and activation of integrins, providing shear stress with a flow chamber to culture the cells is a common method as stimulation for vascular regulation [14-16, 21]. However, cell culture with the devices to apply fluidic shear stress requires a demanding control which includes optimization of flow rate to deliver consistent stimuli. Alternatively, surface modification with nano/micro structure is also known to guide cellular behavior such as cell proliferation, differentiation, and migration [22-25].

Although how topographic modification derives the modulation of cell behavior and function still remains elusive, many research groups have focused on patterning their materials with various geometries for therapeutic use [26-29].Which geometry promotes their cellular responses can be differed by mechanical property of the substrate such as stiffness and cell type. Therefore, designing an appropriate structure to supply physical stimulation to specific cell type for their enhancement is crucial in development of the desired tissue architecture.

Most of all, groove pattern have been mainly used [30-34] as a source to provide geometrically controlled interface with not only endothelial cell but smooth muscle cell (SMC), neuron cell, fibroblast and even

mesenchymal stem cell (MSC) which is also served as ECM. As a result, topographical cues with groove pattern strongly enhanced morphology changes through cellular response. Therefore, incorporating the groove pattern on the substrate has a substantial potential in tissue engineering.

CHAPTER 2.

2.1 Introduction

In this study, we developed the system to delivery endothelial progenitor cell (EPC) overcoming their poor retention for wound healing. It is fabricated based on alginate hydrogel with layer by layer (LBL) technology by electro charge interaction. Magnetic nanoparticle (MNP) is embedded simultaneously during crosslinking of alginate and provides mobility with magnetic force to implant the hydrogel sheet to the wound area. Groove pattern composed of line and space is also incorporated to accelerate cellular response which is essential to prompt vascularization. We evaluated the cell alignment and change of cell morphology by groove pattern on the hydrogel sheet, proliferation rate, differentiation to the endothelial cell, cytokine secretion and further carried out *in vivo* study with mouse subcutaneous wound healing model. Herein, we demonstrated that MNP embedded hydrogel sheet with groove pattern (MPS) induced angiogenesis and vascularization via observation that displays elongated cell shape, enhanced gene expression and up regulated cytokine secretion compared to MNP embedded sheet without pattern (MFS). Further, we also verified a rapid rate of repair of dermal wound by implanting the sheet, encouraging new vessel formation and nourishing the wound area.

2.2 Materials and methods

Preparation of patterned mold

Line : Space = 1:1, 1:3, 1:5 patterned silicon wafer was fabricated with mask-soft lithography method. To obtain positive patterned replica on the pet film, 1st PDMS (Dow corning) replica was prepared at 60°C for overnight. PUA 311 was used with PET film to replicate the pattern on the PDMS. The film replica was stabilized in the UV curing chamber for overnight. .

Fabrication of MNP embedded hydrogel sheet with groove pattern

1.5% (w/v) sodium alginate (FMC biopolymer) was fully dissolved in 0.9% (w/v) sodium chloride (Sigma-Aldrich) at 60°C. 16.67ug/ml concentration of MNP is mixed with alginate solution. Before preparation of the alginate hydrogel, a patterned PET film was attached at the bottom of the 70um pore sized cell strainer (SPL life sciences). 3ml of MNP-alginate solution is poured in the cell strainer and 100mM calcium chloride (Sigma Aldrich) was added outside of the cell strainer to induce polymerization by ion exchange for overnight. In this procedure, a magnet which has 3800gause of magnetic force was placed under the petri-dish to locate MNPs on the desired position. Cross-linked MNP embedded-alginate hydrogel is washed with 0.9% sodium chloride and soaked in 0.1% (w/v)

poly-L-ornithine(PLO) (Sigma Aldrich) in 0.9% sodium chloride for 30minutes. The PLO coated hydrogel then continuously soaked in 5% (w/v) gelatin from bovine skin (Sigma Aldrich) 0.9% sodium chloride for 1 hour. Layer by layered alginate-PLO-gelatin hydrogel is washed and cut to expose alginate and obtain only MNP-patterned area. The section is soaked in 25mM of sodium citrate in distilled water for 3minutes to remove alginate except the part of binding with PLO and hydrogel sheet was fabricated. The sheet was washed with sodium chloride and stored at 4°C.

Z potential measurement

1.5% alginate was coated on LUDOX TM-50colloidal silica particles (Sigma-Aldrich) and its zeta potential of surface was measured by size analyzer (Nanozs, Malvern, Germany). Alginate coated silica particles were then continuously treated with 0.1% PLO and measured, which was followed by the same procedure with 5% gelatin coating on the PLO coated particles.

Synthesis of FITC-alginate, RITC gelatin

The FITC-alginate and RITC gelatin were synthesized for confocal microscopy use. For the synthesis of FITC-alginate, 300mg of sodium alginate was mixed with EDC/NHS(100mg/60mg) in 50ml of DPBS for 30 minutes with stirring. Then, 60mg of Hexamethylenediamine was added and reacted for 4hours. To remove unreacted diamine, precipitation procedure with isopropyl alcohol was done with centrifugation for 15minutes at

3500rpm. 1mg of FITC in pH8.5 sodium bicarbonate solution was further added and reacted for 24hours followed by dialysis at least 4days to discard unreacted FITC with changing the distilled water (DW) every other day. When dialysis was done, the FITC-alginate solution was frozen at -20°C, and lyophilized.

For the synthesis of RITC-gelatin, 5mg of RITC was dissolved in 500ul of DMSO, followed by mixing with 1% gelatin dissolved in DW. The solution was reacted for 1hour at 60°C with shaking and then dialyzed for 4days at the same temperature. Then, the RITC-gelatin was frozen at -20°C, and lyophilized.

Scanning Electron Microscopy

The sheets were completely dehydrated with these procedure; washed with 50% and 70% ethanol (EtOH) balanced with distilled water for 5minutes each, 80% and 95% EtOH for 10 minutes each, and 100% ethanol for 2 x10 minutes followed by drying series with Hexamethyldisilazane (HMDS); washed with the solution of EtOH:HMDS=3:1, 1:1, and 1;3 for 15minutes each, and 100% HMDS until completely dried up. The dried sheets were fixed on the glass and coated with platinum/palladium for 110 seconds. Then, the images were taken by Field emission electron microscopy (FE-SEM; JSM-6701F, JEOL) at 10kV and the surface of patterned hydrogel sheets with/without MNP.

Cell cultures

Human-derived endothelial progenitor cells (hEPCs) were isolated from cord blood and provided from Pusan National University school of Medicine (Pusan, Korea) under prior consent. Before seeding the cells, the sheets were soaked in 70% ethanol for 30minutes, washed with sterile DPBS for 5times and placed in UV chamber for 4hours. 50,000/cm^2 of hEPCs was seeded on the sterilized sheet. All hEPCs used in this study were cultured in endothelial cell medium(Sciencell) which the composition of the solution was 5% fetal bovine serum (Sciencell), 1 % endothelial cell growth supplement (Sciencell), and 1 % penicillin/streptomycin solution (Sciencell) in basal medium (Sciencell). The culture medium was replaced every other day.

Immunocytochemical staining

Cell morphology was analyzed through immunocytochemical staining. 3 x 10^5 cells of hEPCs were seeded per sheets and were incubated for 48 hours. After 48 hours, sheets were washed with DPBS for three times, and fixed with 4% paraformaldehyde for 20minutes. Then remaining PFA was washed with DPBS for 3times and the fixed cells were permeabilized with 0.05% TritonX-100 in 1% BSA/PBS for 20minutes. Followed by another washing step, 2% rhodamin phalloidin (Invitrogen^{TM}) in 1% BSA/PBS for F-actin staining was added and incubated for 1hour at room temperature. After washing them with PBS, the nuclei was stained with

0.5% of DAPI (Vector Laboratories). The images were observed with 20x by the fluorescence microscope (AMF4300 EVOS, Life Technology). On the basis of these images (n = 8), the orientation, length and branching point of the cells were analyzed by using Image J.

Cell viability and cell adhesion test

Live/Dead viability kit (Invitrogen™) was used to observe viability of cells on the sheet. 5×10^5 cells of hEPCs were seeded per sheet which is placed on the 24well. After 24 hours of incubation, each sheets were washed with DPBS and followed by incubation for 20minutes with the solution composed of 500μL of DPBS including 1 μl calcein AM and 0.5 μl ethidium homodimer-1. The viability was measured by the microscope (AMF4300 EVOS, Life Technology).

To observe cell adhesion with the sheets for overnight, Quant-iT™ PicoGreen assay kit (Invitrogen™) was used after Papain digestion (also known as Papaya proteinase Ⅰ) of the attached cells on the sheets. Followed by adding aqueous solution of Quant-iT™ PicoGreen, the amount of DNA was measured by absorbance reader (Infinite 200 PRO TECAN Ltd) (n = 3).

Cell proliferation test

To observe the cell which has potential to proliferate, they were stained with Click-iT Edu Flow Cytometry Assay kits (Invitrogen™) and

the stained cells were analyzed by using image J.

For the measurement of proliferation rate of the cells, they were incubated (n = 3) with Cell counting kit-8 (Dojindo) for 90minutes and their absorbance were read at 450nm of wavelength.

Real time PCR

RNAs were extracted from the cells on the sheets (n = 3) with Trizol (Life Technology) after 3days of incubation. The extracted RNA was reverse-transcribed into cDNA using TOPscript^{TM} Reverse Transcriptase Kit (Enzynomics). Concentration of synthesized cDNA was measured by NanoDrop spectrometer (ND-2000; NanoDrop Technologies) and 200ng of cDNA was used for Real time-PCR, which was performed with ABI StepOnePlus^{TM} real-time PCR system (Applied Biosystems). cDNA was amplified for relative human gene expression of 18s as a housekeeping gene, CD31, VCAM-1, Ve-cadherin5, and PDGFB and the gene expression level was calculated with $-2^{\Delta\Delta Ct}$ method. Primer sequences in RT-PCR were: 18s (Forward: 5'- CCC TGT AAT TGG AAT GAG TCC ACT T-3', Reverse: 5'-ACG CTA TTG GAG CTG GAA TTA C-3'), CD31 (Forward: 5'-AAA TGC TCT CCC AGC CCA GGA T-3', Reverse: 5'-GCA ACA CAC TGG TAT TCG ACG TCT T-3'), VCAM-1 (Forward: 5'-CCC ACA GTA AGG CAG GCT GT-3', Reverse: 5'-GAG CCA CCT TCT TGC AGC TT-3'), Vecadherin-5 (Forward: 5'-ATC AAG CCC ATG AAG CCT CT-3', Reverse: 5'-TGT ATC GGA GGT CGA TGG TG -3'), PDGFB (Forward:

5'-TCG ATC CGC TCC TTT GAT GA-3', Reverse: 5'-GGA ACC CAG GCT CCT TCT TC-3').

Cytokine release

Medium which includes PDGF-BB and VEGF from cultured hEPCs on the sheets was collected on the day1, 2, and 3 and stored at -80°C. The amount of cytokine was measured with ELISA complete kit (KOMABIOTECH) (n = 3) and their absorbance was read at wavelength of 450nm.

In vitro wound healing assay

NIH-3T3 (Korean Cell Line Bank), which is the cell line of was cultured on the 48wells with the general medium which composed of 10% fetal bovine serum (Gibco), 1% L-glutamine (Gibco) in Dulbecco's modified Eagle's medium, until the cells formed a monolayer. To scratch the monolayer, 1000 μL of pipet tips were used and the images were taken immediately after the wounding with the microscope (Olympus). Then, 3types of medium which were defined as normal growth medium, conditioned medium from the each sample with the ratio of 1 : 1 was added to the wounded monolayer. The wound closure was determined based on the analysis of the images (Image J) which were taken 18hours, 22 hours, and 27 hours after scratch.

Mouse subcutaneous wound healing model

Full thickness of wound on the dorsal skin by using biopsy punch with diameter of 8mm was inflicted to balbc nuce mice (6 weeks old, female / Orientbio Co.) (n = 6). MFS/-EPC, MPS/-EPC, MFS/+EPC and MPS/+EPC were implanted with a magnet which was wrapped by parafilm and covered the wound separating from the magnet. For the control group, 200μL of sterile DPBS was added to the wound area. To protect from damage of the vehicles, the area was sealed with Tegaderm (3M) and it was changed every 3 day. The reduction of wound size was identified on the basis of rubber ring and calculated with pixels of the area using image J on the day of 0,3,7,10,14.

Histological analysis

Skin tissues of interest were collected at day7 and 14 and fixed with 4% PFA for 24hours. The tissues were treated with paraffin and sectioned at an appropriate thickness. Sectioned samples were deparaffinated by soaking in series of xylene solution and re-hydrated with EtOH solution. Samples were stained with Hematoxylin and Eosin (H&E) staining and imaged using microscope (Olympus). For the analysis, the length of wound and the number of vessel was measured using Image J. In case of vessel number, it was based on the HPF images of the specific area (20x).

Immunohistochemical staining

Deparaffinated samples were treated with 1x proteinase K solution for antigen retrival and incubated for 10 minutes. After incubation, they were washed with 1%BSA/PBS solution 3times for 5minutes each and permeabilized by the solution which composed of 10% goat serum, 0.1% TritonX-100 in 1% BSA/PBS for 1hour. Primary antibody, CD31, alpha smooth muscle actin (BDscience, Abcam) diluted with the ratio of 1:50, 1:200 in 1% BSA/PBS was treated and incubated for overnight at 4°C. Second antibody solution was prepared with dilution (1:500) and added to the sample on the next day. 2hours after secondary antibody staining, nuclei was stained with DAPI. Images were taken by fluorescent detecting microscope (AMF4300 EVOS, Life Technology) and analyzed with Image J.

Statistical analysis

All data in this paper were expressed with mean ± standard deviation. Statistical significance was determined by one way (or two way) analysis of variance (ANOVA); $^{*}p < 0.05$, $^{**}p < 0.001$, and $^{***}p < 0.0001$.

2.3 Results

Fabrication of MNP embedded hydrogel sheet with groove pattern

To embed MNPs completely inside of the alginate hydrogel, they were homogeneously distributed in alginate solution before crosslinking and located in desired site which contains groove pattern by placing a magnet under the site. After gelation, alginate hydrogel of which MNPs located only

in geometrical center was fabricated and chelated to remove unbound alginate from PLO, when every side of it was exposed to sodium citrate. Maintaining MNPs' position in the cross-linked alginate layer through chelation, MNP embedded hydrogel sheet with pattern was obtained (Figure. 2 A). The structural difference between sheets with MNP or not was observed with SEM imaging (Figure.2 B-C). It is confirmed mobility of the sheets by magnetic force and complete restoration without deformation after bringing it out of water while sheets without MNPs are easy to be torn (Figure.2 D).

Our hydrogel sheet is based on layer by layer-coated by electro charge interaction. At the lowest level of the sheet, alginate which has negative charge (-31.4 ± 1.115mV) is covered with PLO which has positive charge (+31.4 ± 0.3283mV). On the upper level of PLO, gelatin which has slightly negative charge (-3.15 ± 0.46940mV) is coated (Figure.3 A). In addition to z potential analysis to verify layer by layered coating interaction between 3layers, sheets were fabricated with FITC-alginate and RITC-gelatin and imaged with z stack (Figure.3 B). Therefore, we can examine stably bonded layers by electro charge interaction.

Various topography of patterns can be engraved on the hydrogel sheet; line : Space = 1 : 1, 1 : 3, and 1 : 5 of groove patterns(Figure. 4 A) were incorporated within the sheet (Figure. 4 B-D). When EPCs were seeded on these sheets, only 1 : 1 patterned sheet provided micro-environment for cell alignment, which was monitored as a result of F-actin

dapi staining and measurement of the cell orientation (Figure.4 E-J). For further investigation, 1 : 1 pattern was used to develop a system inducing cell alignment.

Characterization of cell morphology on the patterned sheet

EPCs were seeded on TCP, MNP embedded flat sheet (MFS), and MNP embedded patterned sheet (MPS) with the same density of cells. The cells on MPS started to change their morphology while the cells on TCP, and MFS maintained their morphology as cobble stone shape (Figure.5 A). MPS induced cell alignment with highly uniform orientation distribution compared to MFS (Figure.5 B-C). The number of branching point which is expressed as a start point to be spilt into several strands was counted based on the images and MPS presented much higher number of branching points (Figure.5 D). In addition, measuring the length of cells, MPS displayed the most elongated cell shapes compared to other groups (Figure.5 E)

Cell viability and adhesion analysis

Viability of cells on the TCP, MFS, and MPS was tested to investigate cytotoxicity of the sheets. After incubation for 24hours, fluorescence detecting imaging was performed to determine live (green) and dead (red) cells. As a result, all groups showed cell viability over 95% (Figure.6).

Cell adhesion to the sheets was analyzed by DNA quantification

after incubation for 18hours. The DNA concentration of MFS and MPS was normalized with the concentration of TCP. Slightly higher cell adhesion to the MPS (94.44 ± 3.813%) was observed, but there was no significant difference with MFS (92.96 ± 2.350 %) (Figure.7).

Cell proliferation analysis

For measurement of cell's ability to proliferate, the cells in S phase were stained with EDU (green) after 48 hours of incubation and quantified based on images. % of green cells of MPS was 28.59 ±3.303%, which is comparable with TCP (29.25 ±2.483%). However, MFS showed significantly low % concentration (19.51 ±0.7196%) of the cells which have potential for proliferation (Figure.8 A)

In addition, CCK-8 assay was done to measure cell proliferation rate in a time dependent manner. The result indicated that MPS enhanced the proliferative ability by surpassing TCP group on day3 (Figure. 8 B).

Enhanced differentiation to endothelial cells

Verifying differentiation of endothelial progenitor cells into endothelial cell and their maturation, genes in the cells on the TCP, MFS, MPS was amplified using RT-PCR after 3days of culture. Relative gene expression was measured with angiogenesis markers such as CD31, VCAM-1, Ve-cadherin5, and PDGFB. As a result, MPS exhibited much enhanced gene expression in all markers compared to other groups while there was no

significant difference of gene expression between TCP and MFS (Figure. 9).

In vitro wound healing

Cytokine secretion from cells on TCP, MFS and MPS in time dependent manner was detected with ELIZA kit. It was indicated that MPS group enhanced the release of growth factors such as PDGF-BB and VEGF from cells compared to others. However, VEGF release of MPS presented only small amount of increase without any significance among other groups (Figure.10).

To determine how growth factors from cells on MFS and MPS influenced on migration of fibroblast, *in vitro* wound healing assay was done with conditioned medium which is composed of 50% of culture medium from MFS or MPS after 3days of incubation and 50% of fibroblast general growth medium. 27 hours after scratch and adding conditioned medium each, only MPS exhibited complete closure of wound area (Figure.11)

Local delivery of sheet & In vivo wound healing

For highly efficient local delivery, a sterilized magnet wrapped with parafilm was used to move the sheets (MFS, MPS, MFS/EPC, MPS/EPC) out of medium. Then, the sheets were detached from parafilm and delivered to wound area which was punched with biopsy punch (Figure.12 A). Reduction of wound area was calculated on the basis of the images

(Figure.12 B-C). EPC positive groups (MFS/EPC, MPS/EPC) exhibited rapid recovery compared to EPC negative groups (TCP, MFS, MPS). However, 7 days after surgery, recovery rate of MFS/EPC started to be slow than MPS/EPC. On day 14 post wounding, the wound on which MPS/EPC was delivered remained as more receded and smaller scar than MFS/EPC implanted group.

In addition, the area of vessel formation surrounding the wound was evaluated after collecting skin on day 7 and 14 (Figure.13). The result of measuring total vessel sprouting area indicated that MPS/EPC showed the most improved vessel formation. Interestingly, overall sprouting area of every group on day 14 was slightly lower than on day 7.

Histology evaluation

Through histological analysis of H&E staining, granulation tissue formation and reduction of wound length by tracing normal epidermis can be observed (Figure. 14, 15). Also, several blood vessels with interposed red blood cells were found on the basis of HPF image analysis. 7days after implantation, MPS/EPC presented the most shortened wound length, but there was no significant gap among MPS, MFS/EPC. However, plenty of vessel numbers were quantified in MPS/EPC implanted group compared to other groups (Figure. 14 B-C). With the same tendency regarding wound length and vessel numbers between day 7 and day 14, the result indicated that MPS/EPC most enhanced reduction of wound length and formation of

vessel, which was much lower than day 7 however (Figure. 15 B-C). Further, the H&E stained images on day 14 generally focused on exhibiting remodeled skin tissue which can be described as regeneration of epidermis and follicle hair.

Confirmation of vascularization in vivo

Vascularization was demonstrated via immunohistochemistry targeting CD31 antibody which is the most common surface marker of endothelial cell and alpha smooth muscle cells (α-SMCs). As a result of staining with CD31 (red), long stretches of connected antibodies were mostly detected in MFS/EPC, MPS/EPC, while the other groups showed individually distributed antibodies (Figure. 16 A). Evaluating fluorescence and area of CD31, MPS/EPC implanted group indicated the most enhanced fluorescence level and expanded CD 31 positive area (Figure. 16 B-C). Through quantification of α-SMCs, the number of vessels were counted and significantly higher density of vessel was found in MPS/EPC group (Figure. 17).

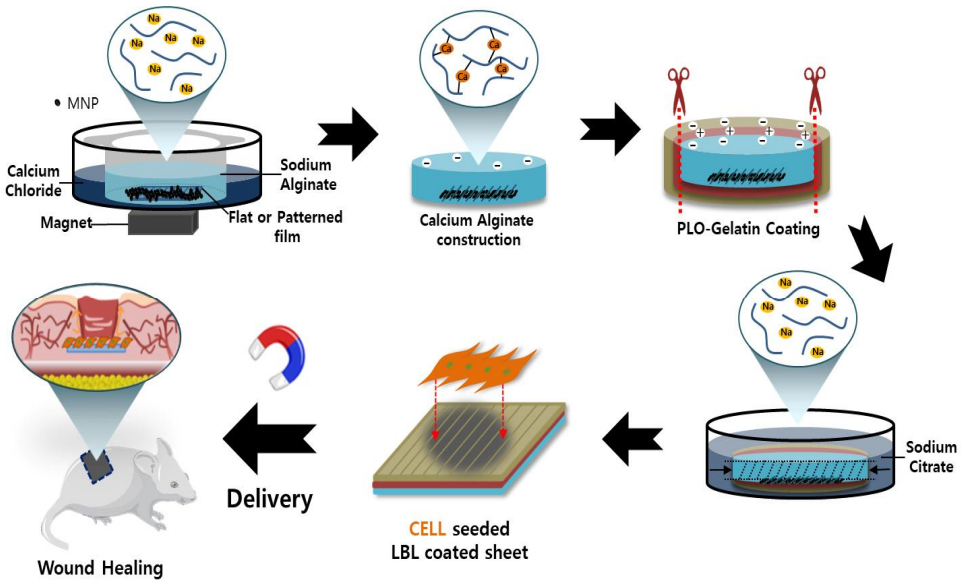

Figure 1. Scheme for synthesis of MNP embedded hydrogel sheet with groove pattern for wound healing.

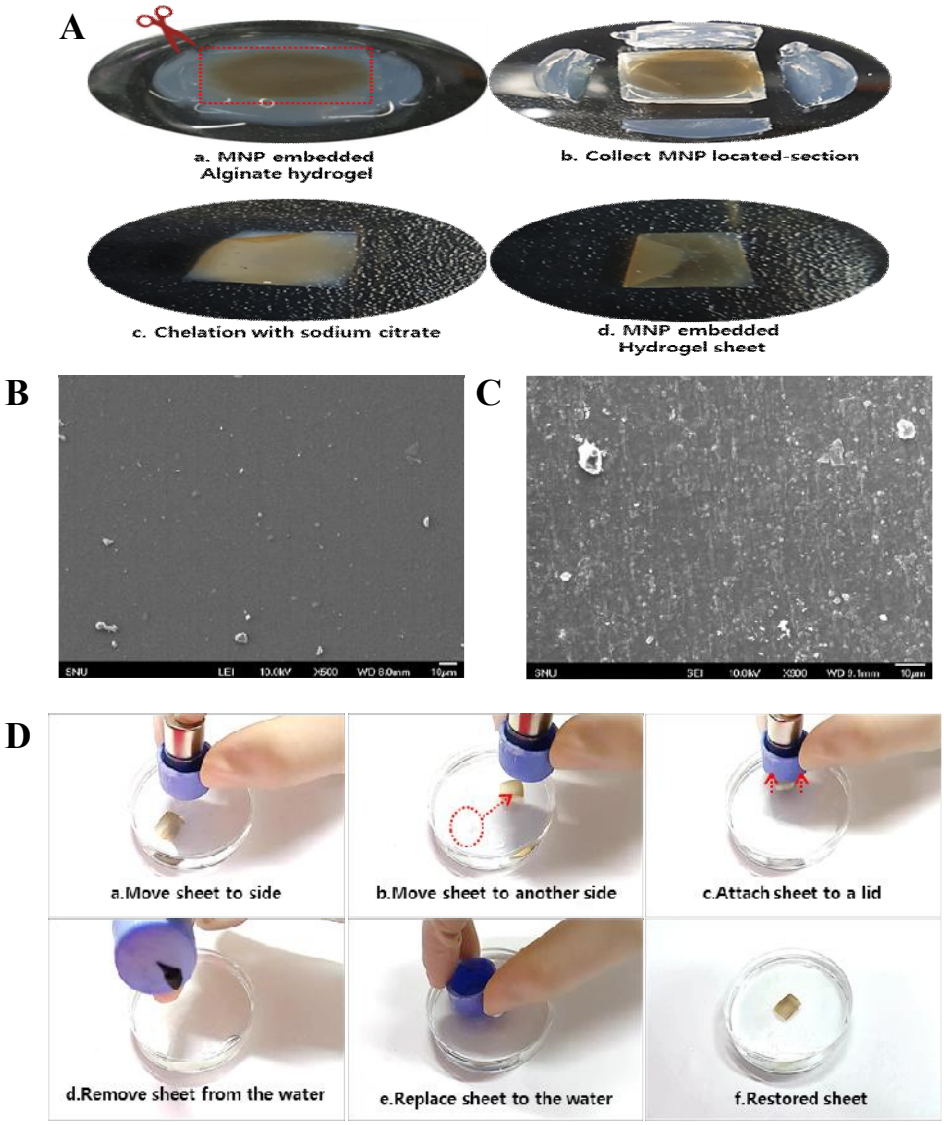

Figure 2. Characterization of MNP embedded sheet (A) Procedure of MNP embedded sheet, (B) SEM image of the hydrogel sheet without MNP, (C) with MNP, (D) Captured images from video showing mobility of MNP embedded sheet along with magnet.

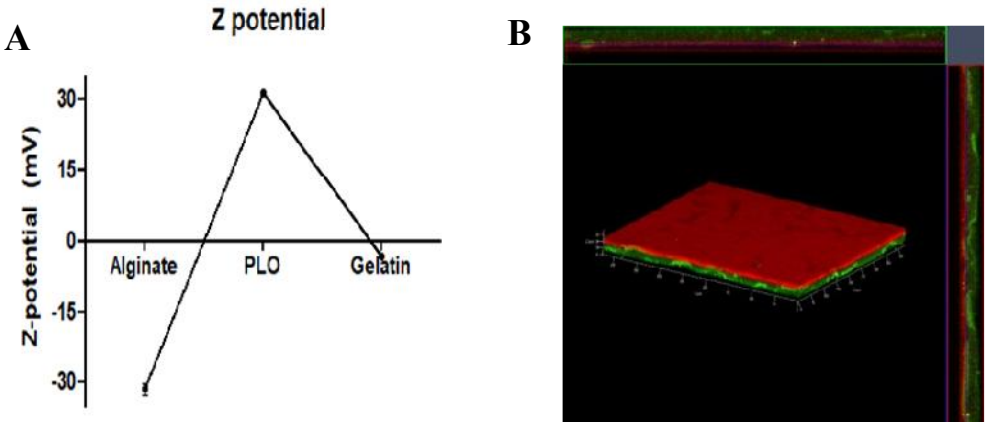

Figure 3. Characterization of Layer-by-Layered coated sheet (A)Z-potential values of alginate and layer-by-layer coated with plo and gelatin, (B) Confocal image of the layer-by-layer coated sheet.

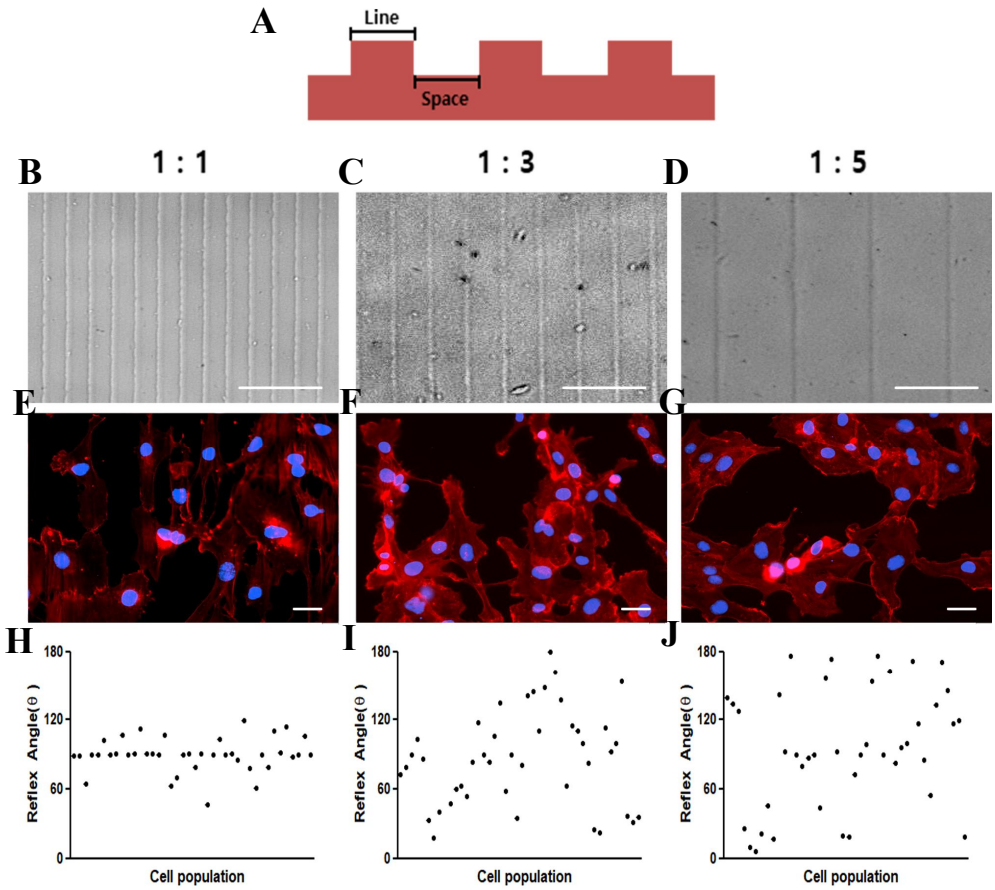

Figure 4. Characterization of hydrogel sheets with various groove patterns (A) Cross-sectional structure of groove pattern, (B)-(D) Bright field images of the sheets with groove pattern of Line : Space = 1 : 1, 1 : 3, 1 : 5. Scale bar = 50 μm, (E)-(G) F-actin/Dapi stained Images of the cells on the patterned sheets each, (H)-(J) Quantification of cell orientation (n = 40) , Scale bar = 50 μm.

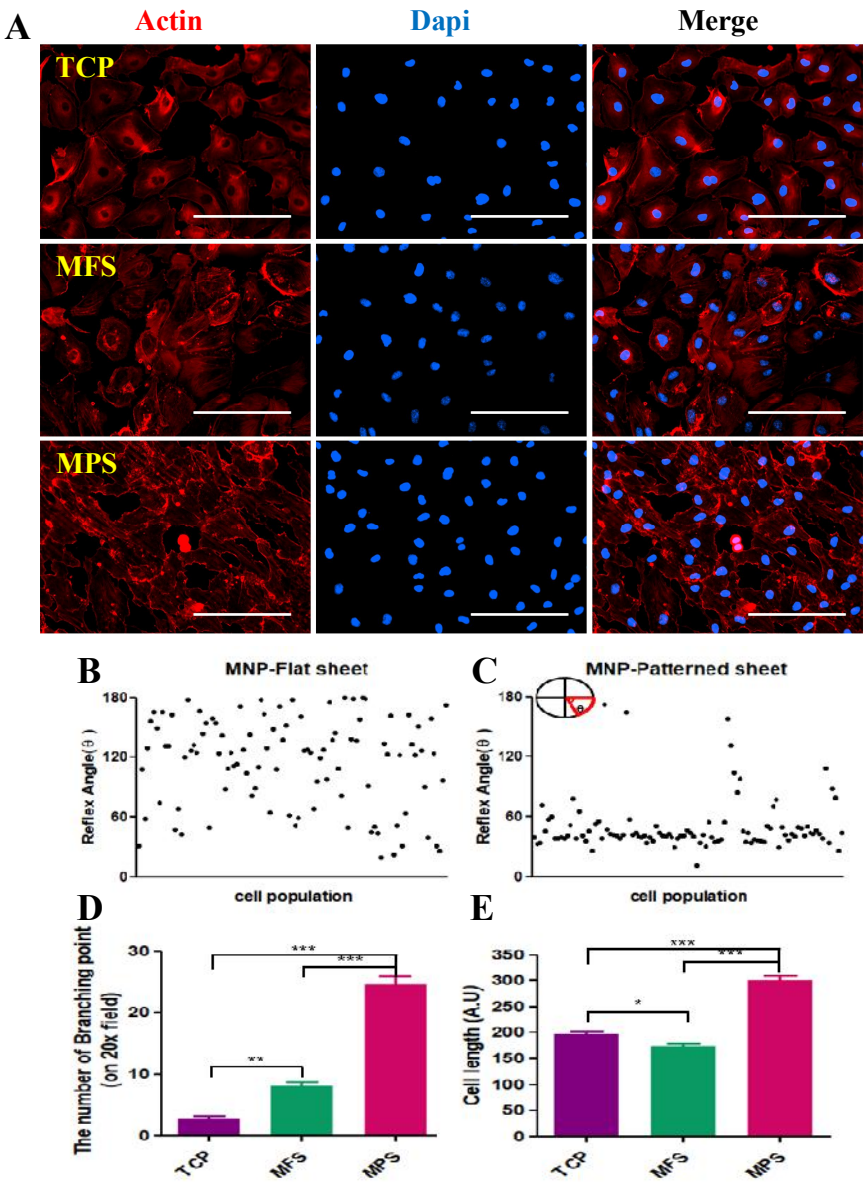

Figure 5. Characterization of cell morphology (A) Representative images of F-actin & Dapi stained cells on the TCP, MFS, MPS, (B)-(C) Cell distribution based on cell orientation (n = 200), (D) Quantifying the number of branching point based on 20x field images (n = 6), (E) Quantifying the length of each cells (n = 60). **p*-value<0.05, ***p*-value<0.001, ****p*-value<0.0001, Scale bar = 200 μm.

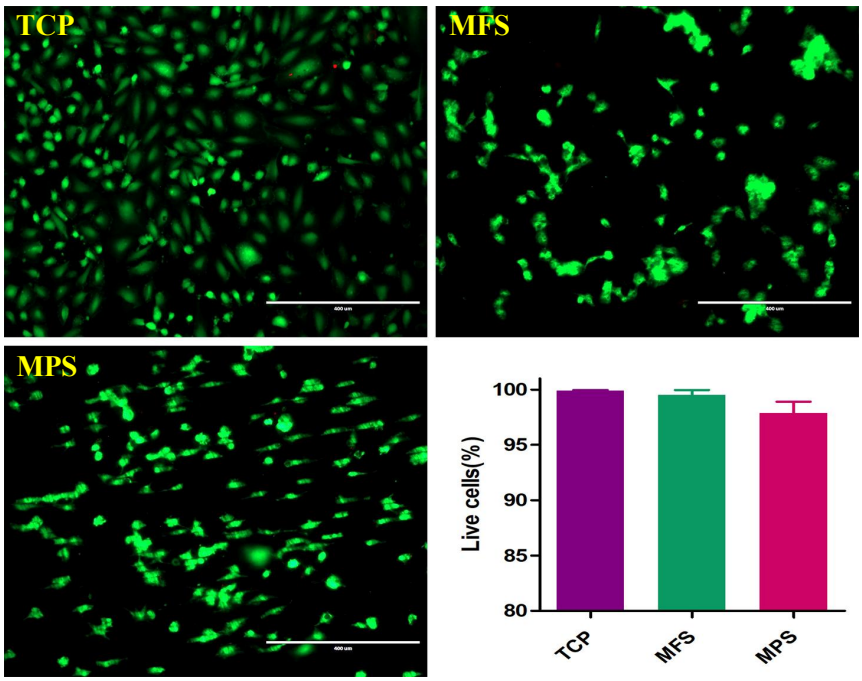

Figure 6. Live & Dead assay for confirming biocompatibility of the MFS, MPS (n = 3).

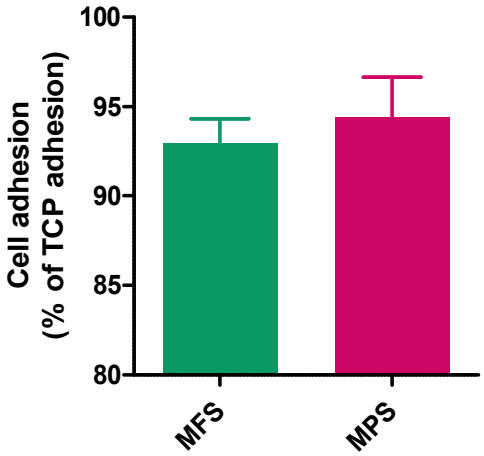

Figure 7. Cell adhesion ratio of MFS and MPS comparing with the TCP (n = 3).

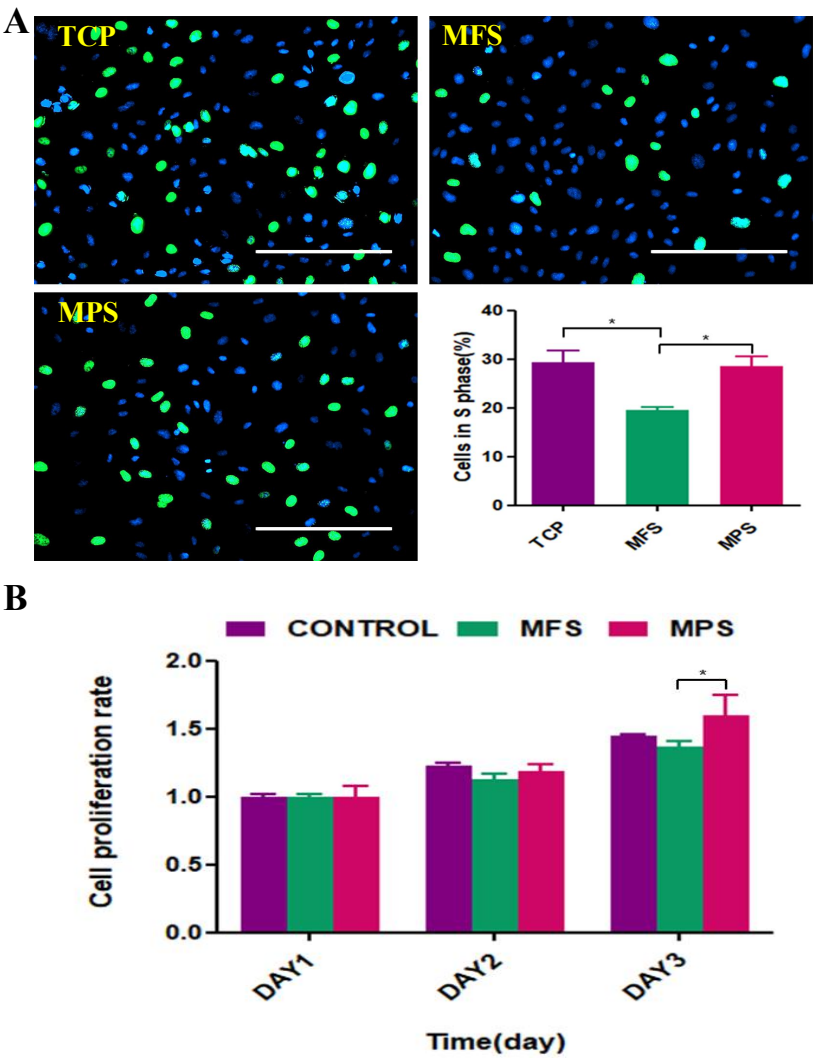

Figure 8. Cell proliferation assay (A) EDU staining and quantification of the number of cells in S phase (n = 3), (B) Cell proliferation rate from cck-8 assay on day 1,2 and3 (n = 3). *p-value<0.05, Scale bar = 200 μm.

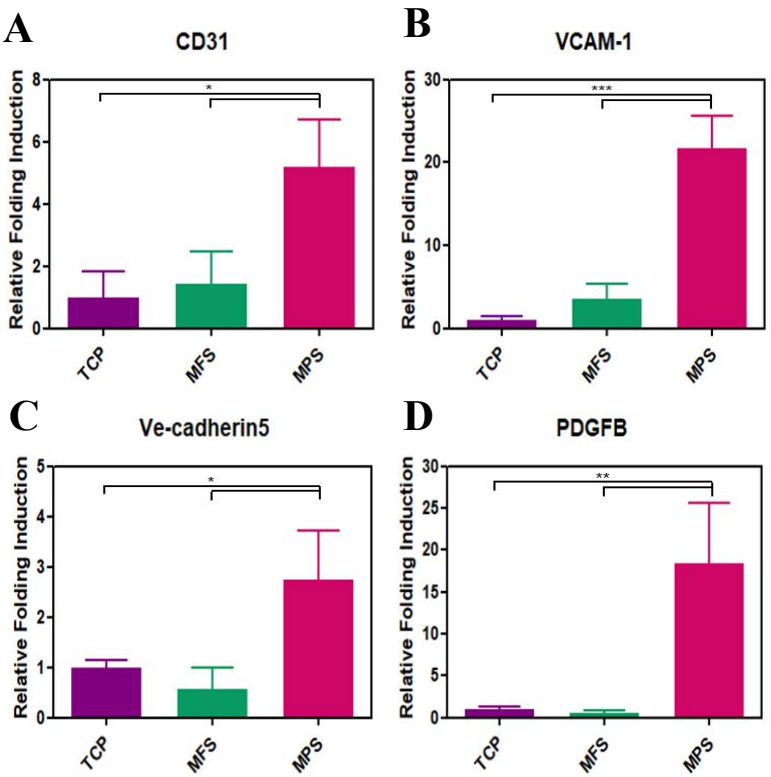

Figure 9. Endothelial differentiation of endothelial progenitor cells on the TCP, MFS, MPS (A) relative gene expression of CD31 (n = 3)**,** (B) VCAM-1 (n = 3)**,** (C) VE-cadherin-5 (n = 3)**,** (D) PDGFB (n = 3)**.**

**p*-value<0.05, ***p*-value<0.001, ****p*-value<0.0001.

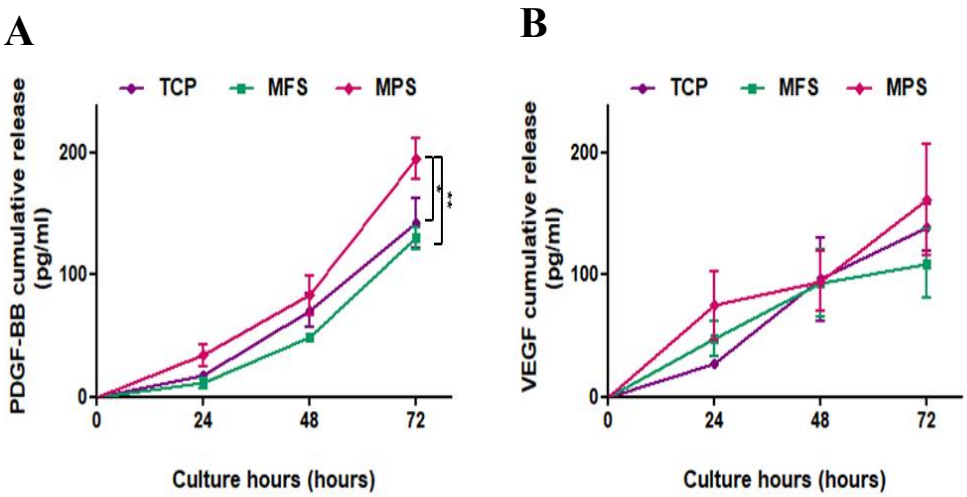

Figure 10. Cumulative release of cytokine from EPCs (A) PDGF-BB release from EPCs on the TCP, MFS, and MPS (n = 3)**,** (B) VEGF release from EPCs (n = 3). **p*-value<0.05, ***p*-value<0.001, ****p*-value<0.0001.

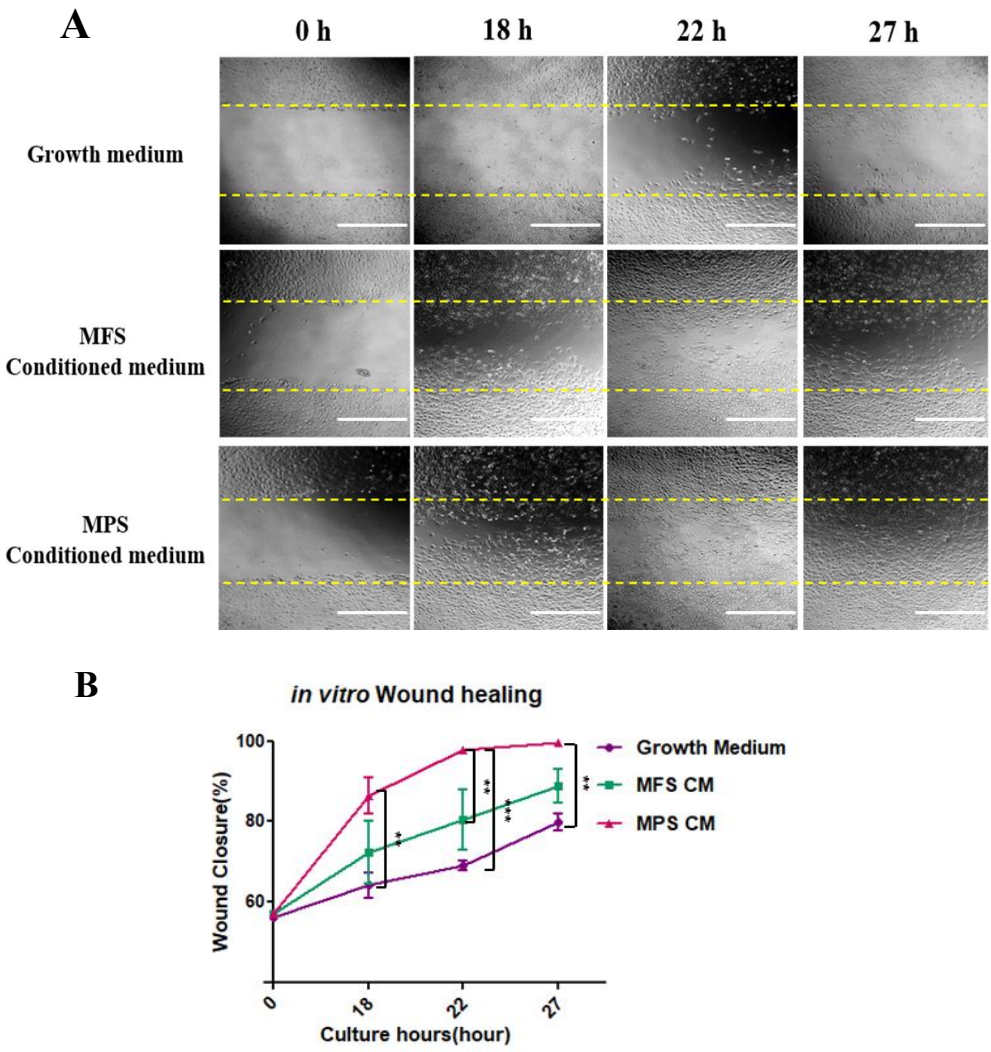

Figure 11. *In vitro* wound healing assay (A) Bright field images to confirm in vitro wound healing rate at the time point; 0h, 18h, 22h, and 27h, (B) Quantification of the wound closure rate (n = 3), **p*-value<0.05, ***p*-value<0.001, ****p*-value<0.0001, Scale bar = 400μm.

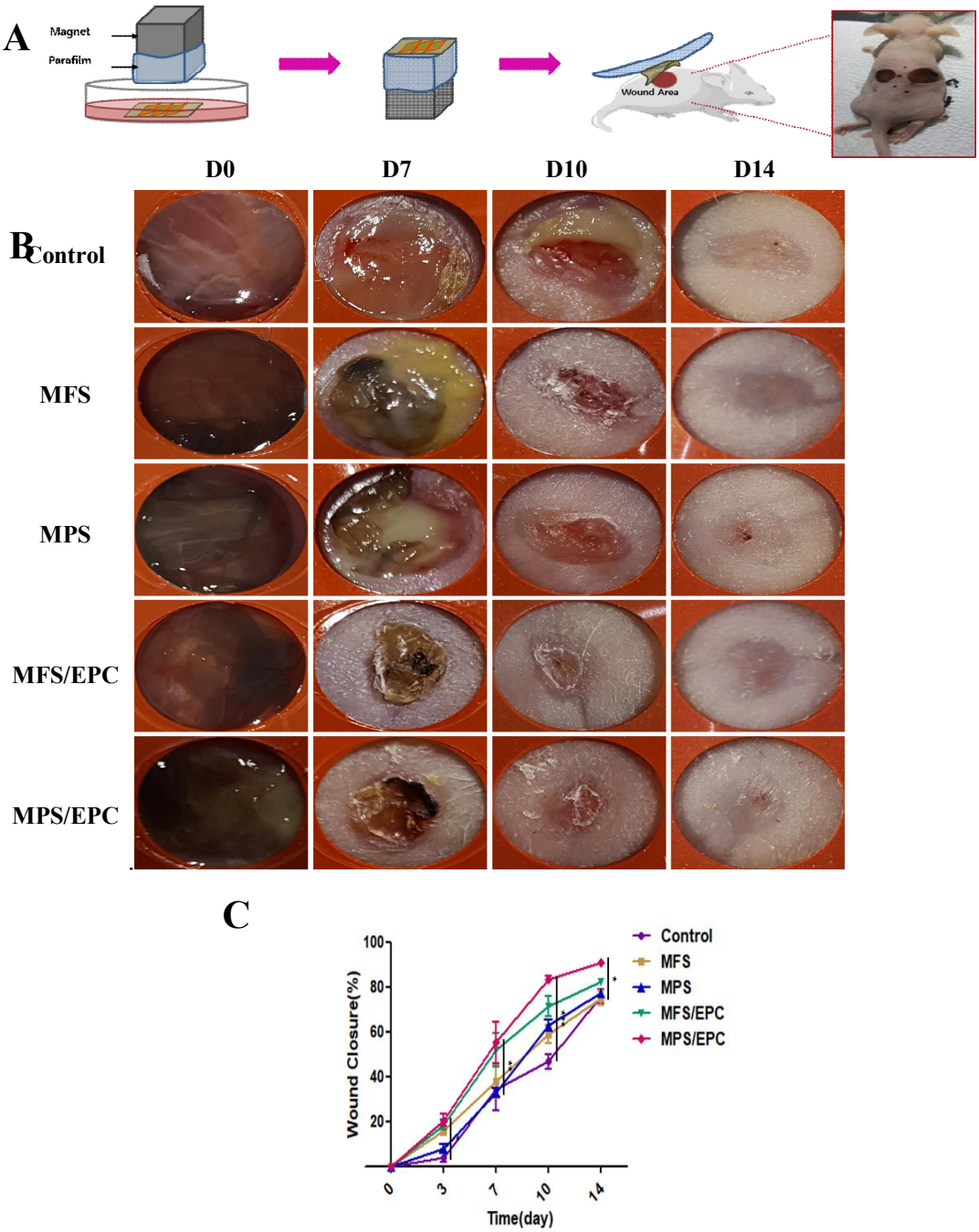

Figure 12. *In vivo* wound healing (A) Scheme of implantation of the sheets, (B) Images of wound closure at the time point; day0, 7, 10, and 14 (n = 6), (C) Quantification of wound closure rate. **p*-value<0.05, ***p*-value<0.001, ****p*-value<0.0001.

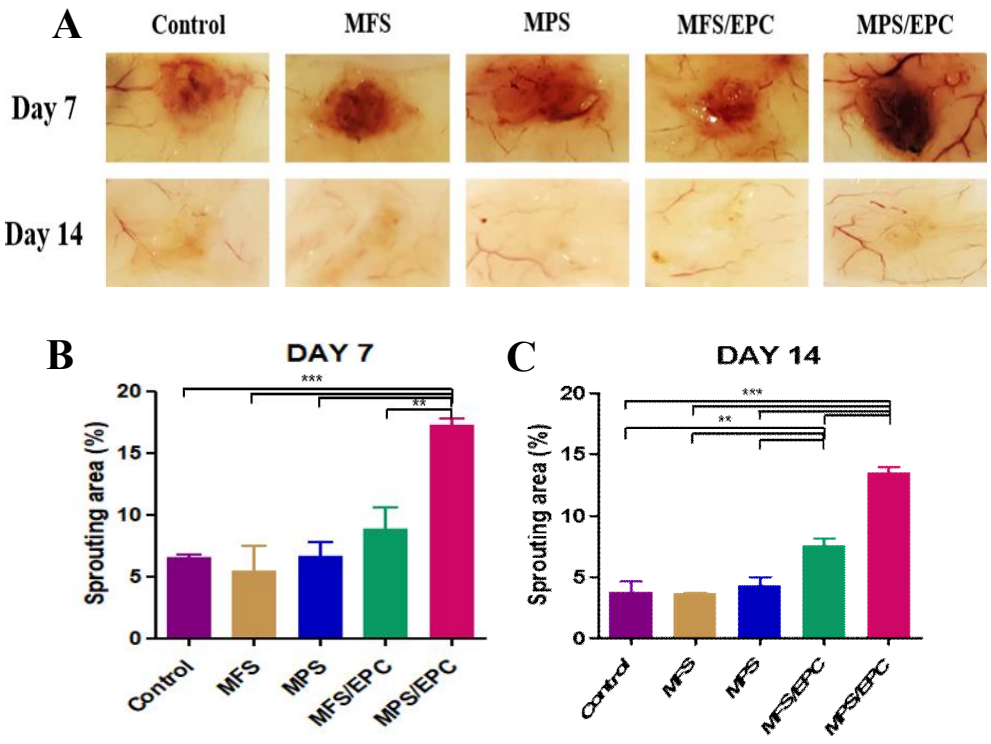

Figure 13. Vessel formation (A) Representative actual images of vessels surrounding wound area, (B)- (C) Quantification of vessel sprouting area of total area on 7 day and 14 day post wounding (n = 3), **p*-value<0.05, ***p*-value<0.001, ****p*-value<0.0001.

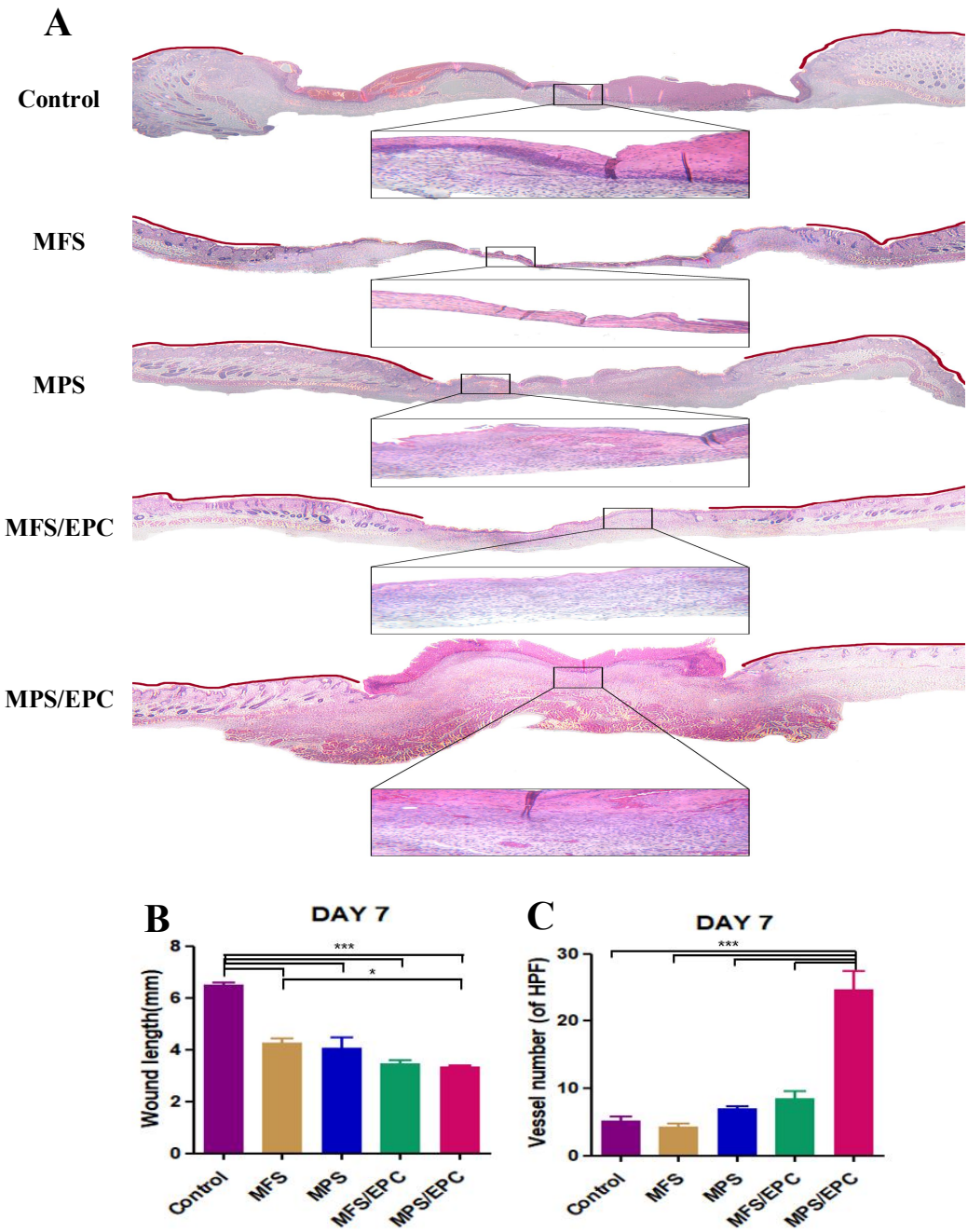

Figure 14. Histological analysis of H&E 7days after surgery (A) Representative images of H&E staining,(B) Quantification of wound length(n = 3), (C) Quantification of the number of vessels based on HPF(20X) images (n = 6). **p*-value<0.05, ***p*-value<0.001, ****p*-value<0.0001.

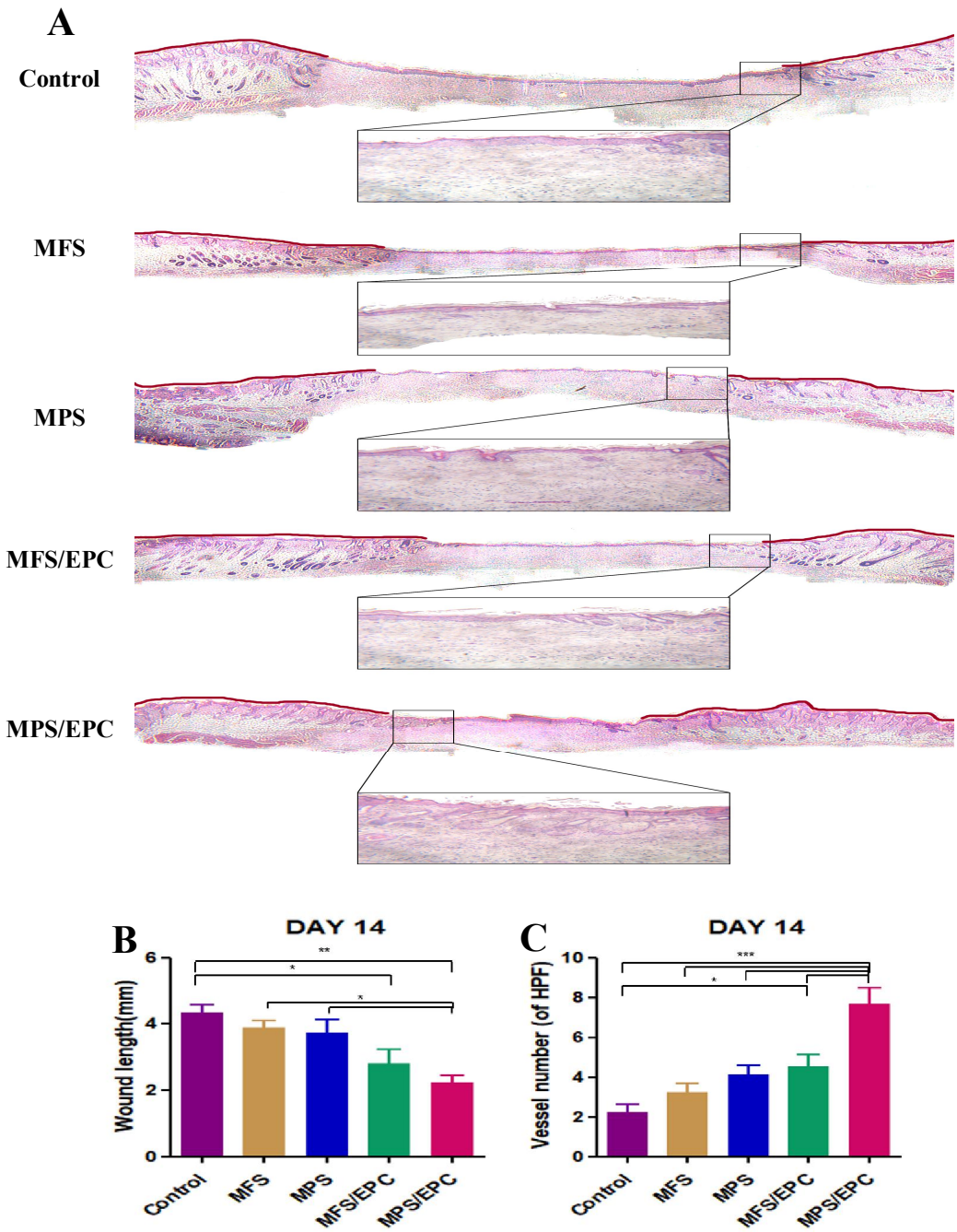

Figure 15. Histological analysis of H&E 14days after surgery (A) Representative images of H&E staining, (B) Quantification of wound length(n = 3), (C) Quantification of the number of vessels based on HPF(20X) images(n = 6).*p-value<0.05, **p-value<0.001, ***p-value<0.0001.

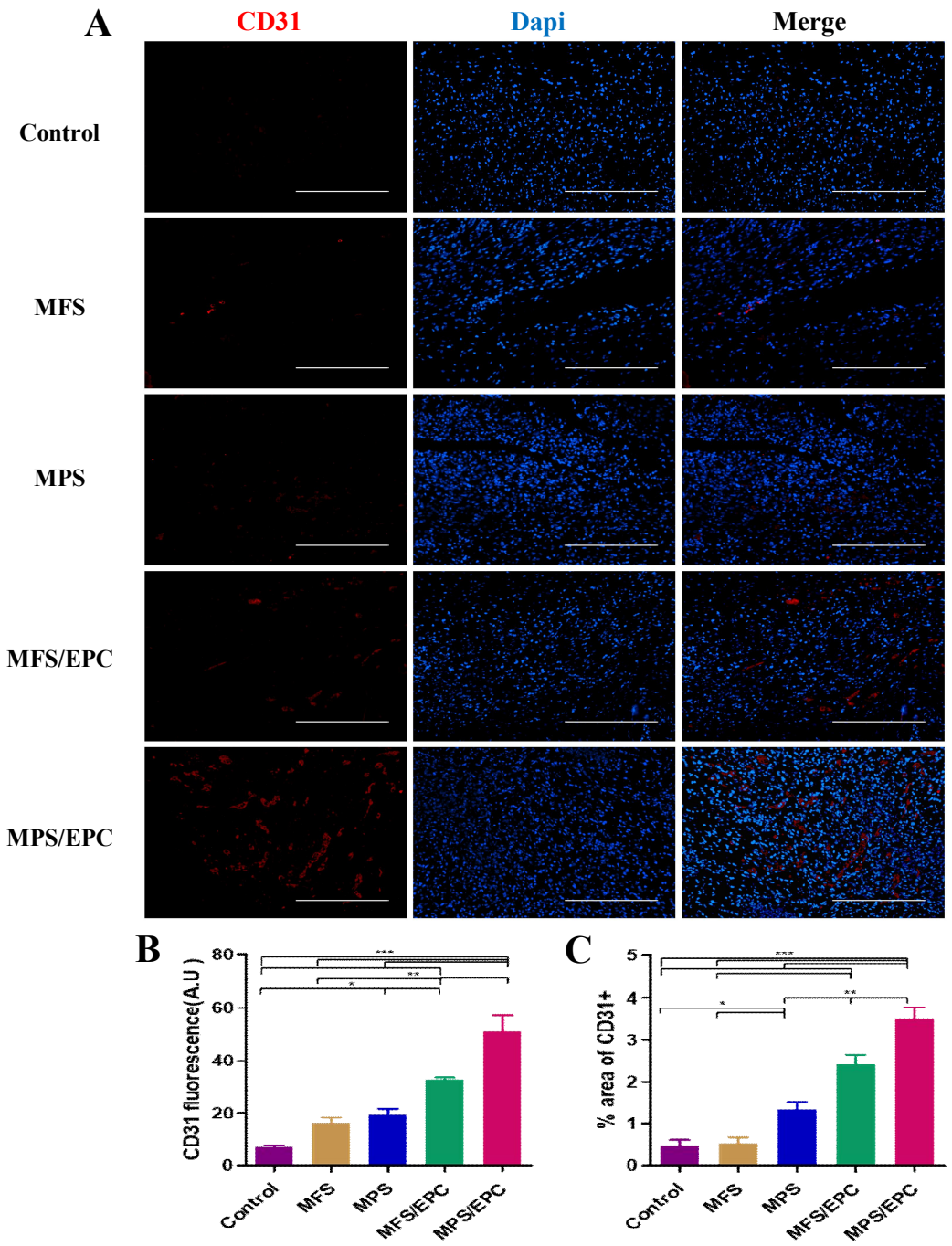

Figure 16. Immunohistochemistry of CD31 7days after surgery (A) Representative images of CD31 staining, (B) Quantification of CD31 fluorescence intensity, (C) Calculation of CD31+ area per total area. (n = 3), **p*-value<0.05, ***p*-value<0.001, ****p*-value<0.0001, Scale bar =200 μm.

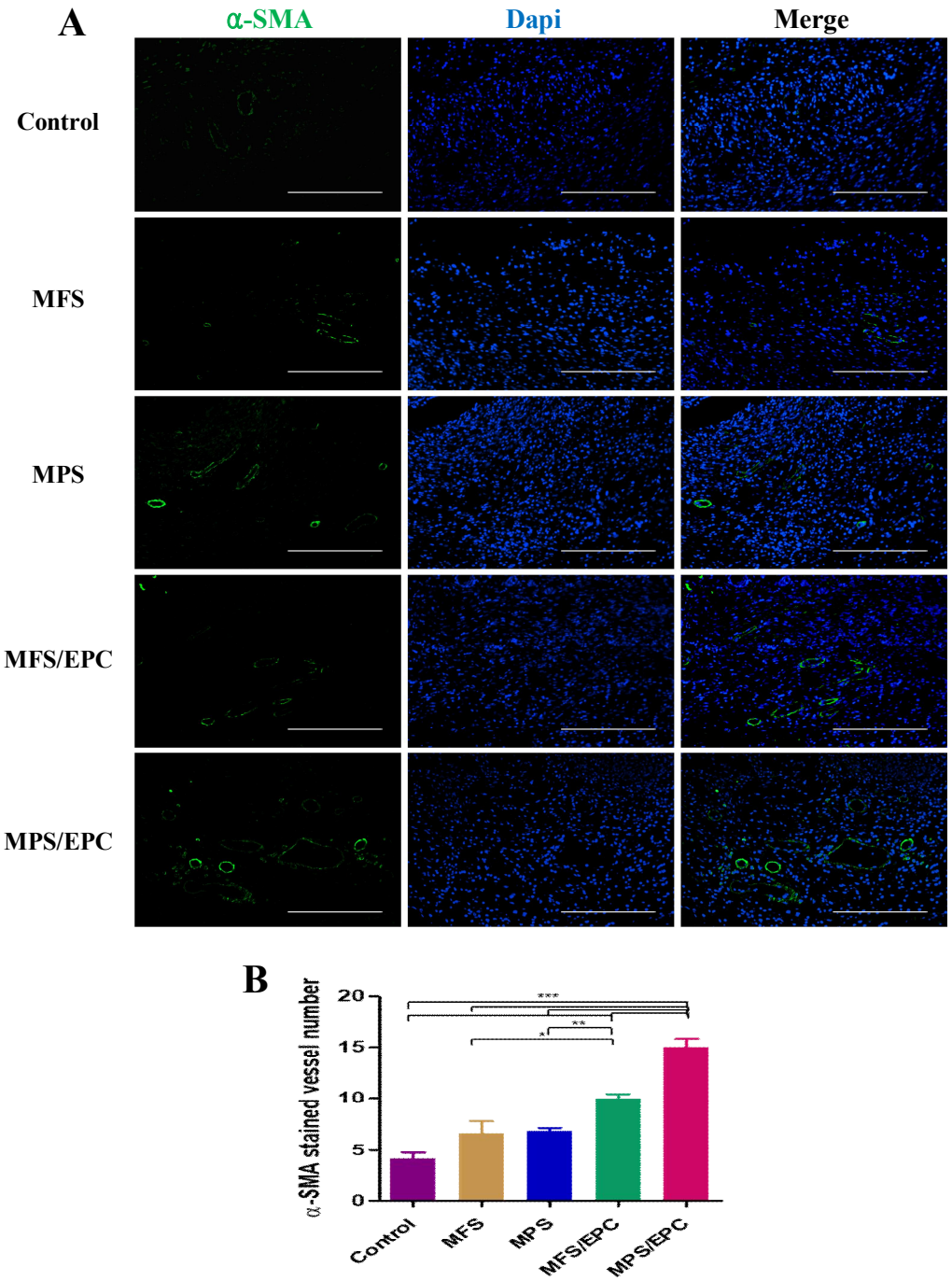

Figure 17. Immunohistochemistry of α-SMA 7days after surgery (A) Representative images of α-SMA staining, (B) Quantification of vessel number. (n = 5)*p-value<0.05, **p-value<0.001, ***p-value<0.0001, Scale bar = 200 μm.

2.4 Discussion

Alginate hydrogel which can be simply cross-linked by ion exchange with calcium is a desired injectable material due to its anti-thrombogenic property compared to other materials [35]. However, its ability to interact with cells is limited, so it is needed to be modified to increase cellular interaction for tissue repair [36]. Mostly, alginate is modified with conjugation of RGD peptide, but we established alteration of the substrate as gelatin derived collagen, which is the most abundant composition of ECM via layer by layer (LBL) technology. To realize employment of LBL method, biocompatible polymer, PLO which has positive electro charge is commonly used to be bound to alginate by electro charge interaction [37]. Since PLO can also mediate the interaction with gelatin which has negative charge, the surface of PLO can be altered with gelatin (Figure. 3). At the end of these procedures, unbound alginate from PLO was eliminated via simple exposure to sodium citrate, which remove cross-linked network with calcium ion. In this way, alginate hydrogel based layer by layer sheet which has a great affinity with cells was developed.

Topographical modification with groove pattern was used to mimic native tissue which is severely influenced by blood flow. In native tissue, endothelial cells are aligned and elongated unidirectionally, being influenced shear stress by blood flow. Then they start to maturate forming several branches and lumens, and establish vasculature [38]. Endothelial

progenitor cells on the surface of Line : Space = 1 : 1 enhanced cell alignment and elongation which plays an important role in endothelial functioning while morphology of other groups tended to display cobble stone shape or without alignment (Figure. 4) Therefore, 1 : 1 pattern was used for further investigation for evaluate their ability to stimulate cellular behavior in this paper. EPCs on MPS tend to form not only more branches but connection with cells like native blood vessel (Figure. 5). Therefore, we hypothesized that topographical modulation triggers differentiation of endothelial progenitor cells into endothelial cells, maturation of endothelial cells, and activation of cytokine secretion for vascularization based on cytoskeleton changes which usually appear on the effect of shear stress in native endothelium. For demonstration of this hypothesis, various assays had been enacted in this paper.

Regulating mechanical stiffness of the substrate to culture healthy cells is a major factor for designing a construction to induce tissue repair and the degree of rigidity depends on materials, cell type or any other environmental element [39-41]. However, our system based on hydrogel sheet had a limit on providing an appropriate microenvironment with enough stiffness, which may explain why MFS, the plain model of hydrogel sheet exhibited inferior cell behavior compared to other groups. Building more layers on the top of other layer with LBL method by electro charge interaction could be another option to augment mechanical property. Instead, we suggested inducing mechanical signals via patterning the substrate as an

efficient alteration not only to modulate cytoskeleton but to overcome the weakness of our system. Cell shape is revised as a response of tension through an interaction with ECM, and adjacent cells. Further, the interaction also effects on cell focal adhesion and functionality of cells including cell proliferation [42, 43]. In accordance with this theory, our strategy with the modification (MPS) was verified as a remedy improving cell-substrate attachment and proliferation which is corresponding to culture on TCP (Figure. 7-8).

Differentiation of EPC into endothelial cells and enhancement of vascularization/ angiogenesis were verified with real time PCR method. E Trizma et al. investigated applying mechanical stimulation such as shear stress induces upregulation of platelet endothelial cell adhesion molecule (CD31), vascular cell adhesion molecule (VCAM-1), vascular endothelial cadherin (Ve-cadherin5), and platelet derived growth factor (PDGFB) [16]. CD 31, which is also known as PECAM-1, is defined as the first activated molecule in response to mechanical stress and promotes mechano-signal transduction in endothelial cells [44, 45]. However, downregulation of these genes occurs when it is exposed to continuously laminar flow, consistent force infliction. Our system which triggers mechanical signal to cell from topographical modification presented enhancement of all gene expression with stimulation of 3 days. Further, we suggest that MPS encouraged differentiation of EPCs, thereby identifying amplification of the endothelial gene marker (Figure. 9). In addition, the ability of cytokine release was

evaluated and EPCs on MPS secreted significantly increased amount of PDGF-BB compared to other groups. PDGF-BB is mainly released from endothelial tip cell which tend to be formed after maturation of endothelial cell. Therefore, stimulation of maturation with groove pattern of MPS enhanced PDGF-BB secretion (Figure. 10).

In wound healing process, the capability of provoking cell migration into the wound area need to be the first requirement. The culture medium from MFS/EPC, MPS/EPC which contained cytokines such as PDGF-BB and VEGF was added to fibroblast culture to study the impact of growth factors on cell migration *in vitro*. From the effect of augmented growth factor secretion, the medium from MPS/EPC contributed to accelerate the wound closure (Figure. 11).

Based on *in vitro* results, hydrogel sheets were implanted 3 days after culture. For the delivery, sterilized magnet was used to move the sheets without deformation. Without magnetic force, it is infeasible to remove them out of medium as their original shapes since they are vulnerable to physical operation out of water. Following the surgery, wound closure rate and newly formed vessel area of skin was measured. MPS/EPC had the most rapid closure of wound consulting the smallest scar and improved vessel formation while MFS/EPC left much bigger scar (Figure. 12-13). Furthermore, analyzing H&E staining on day7, 14, the most shrunken wound length and the highest density of vessel formation was found in MPS/EPS group. Implantation of MPS/EPC promoted vascularization in

wound area, and nourished the injured site with oxygen and growth factors through blood, which helped the rapid treatment.

For closer investigation of blood vessel formation of wound area, immunohistochemistry targeting CD31 and α-SMA was conducted and the highest level of CD31, α-SMA was stained in MPS/EPC group. Considering the result of *in vitro*, MPS/EPC contributed to vascularization and further rapid treatment for dermal wound.

CONCLUSION

In this study, we introduce magnetic nanoparticle embedded hydrogel sheet with groove pattern which was synthesized via layer by layered coating method as a cell delivery tool for tissue repair. We also suggest that our topographically modified system promoted not only differentiation of EPCs into endothelial cell, but also cellular behavior including cell proliferation, maturation and alignment like native tissue. Furthermore, these cellular responses result in enhanced angiogenesis/vascularization of the target site which requires to be nourished such as wound. Thus, by improving endothelial cell functionality and cell retention, our system has considerable potentials as a therapeutic application for tissue regeneration.

REFERENCE

1. Takeo, M., W. Lee, and M. Ito, *Wound healing and skin regeneration.* Cold Spring Harb Perspect Med, 2015. **5**(1): p. a023267.
2. Eming, S.A., P. Martin, and M. Tomic-Canic, *Wound repair and regene ration: mechanisms, signaling, and translation.* Sci Transl Med, 2014. **6** (265): p. 265sr6.
3. El-Sherbiny, I.M. and M.H. Yacoub, *Hydrogel scaffolds for tissue engin eering: Progress and challenges.* Glob Cardiol Sci Pract, 2013. **2013** (3): p. 316-42.
4. Carmeliet, P., *Angiogenesis in life, disease and medicine.* Nature, 2005. **438**(7070): p. 932-6.
5. Gnecchi, M., et al., *Paracrine mechanisms in adult stem cell signaling and therapy.* Circ Res, 2008. **103**(11): p. 1204-19.
6. Hristov, M. and C. Weber, *Endothelial progenitor cells: characterization, pathophysiology, and possible clinical relevance.* J Cell Mol Med, 20 04. **8**(4): p. 498-508.
7. Rehman, J., et al., *Peripheral blood "endothelial progenitor cells" are derived from monocyte/macrophages and secrete angiogenic growth factors.* Circulation, 2003. **107**(8): p. 1164-9.
8. Urbich, C., et al., *Soluble factors released by endothelial progenitor c ells promote migration of endothelial cells and cardiac resident proge nitor cells.* J Mol Cell Cardiol, 2005. **39**(5): p. 733-42.
9. Zisch, A.H., *Tissue engineering of angiogenesis with autologous endot helial progenitor cells.* Curr Opin Biotechnol, 2004. **15**(5): p. 424-9.
10. Wang, C., et al., *Highly efficient local delivery of endothelial progenit or cells significantly potentiates angiogenesis and full-thickness woun d healing.* Acta Biomater, 2018. **69**: p. 156-169.
11. Suh, W., et al., *Transplantation of endothelial progenitor cells accelera tes dermal wound healing with increased recruitment of monocytes/ macrophages and neovascularization.* Stem Cells, 2005. **23**(10): p. 157 1-8.
12. Kwon, Y.W., et al., *N-Acetylated Proline-Glycine-Proline Accelerates Cut aneous Wound Healing and Neovascularization by Human Endothelial Progenitor Cells.* Sci Rep, 2017. **7**: p. 43057.
13. Kim, B.S., et al., *3D cell printing of in vitro stabilized skin model and*

in vivo pre-vascularized skin patch using tissue-specific extracellular matrix bioink: A step towards advanced skin tissue engineering. Biomaterials, 2018. **168**: p. 38-53.

14. Pierce, G.F., et al., *Role of platelet-derived growth factor in wound healing.* J Cell Biochem, 1991. **45**(4): p. 319-26.
15. Azuma, N., et al., *Role of p38 MAP kinase in endothelial cell alignment induced by fluid shear stress.* Am J Physiol Heart Circ Physiol, 2001. **280**(1): p. H189-97.
16. Tzima, E., et al., *A mechanosensory complex that mediates the endothelial cell response to fluid shear stress.* Nature, 2005. **437**(7057): p. 426-31.
17. Liu, J. and S. Agarwal, *Mechanical signals activate vascular endothelial growth factor receptor-2 to upregulate endothelial cell proliferation during inflammation.* J Immunol, 2010. **185**(2): p. 1215-21.
18. Myers, K.A., et al., *Distinct ECM mechanosensing pathways regulate microtubule dynamics to control endothelial cell branching morphogenesis.* J Cell Biol, 2011. **192**(2): p. 321-34.
19. Norton, K.A. and A.S. Popel, *Effects of endothelial cell proliferation and migration rates in a computational model of sprouting angiogenesis.* Sci Rep, 2016. **6**: p. 36992.
20. Gaengel, K., et al., *Endothelial-mural cell signaling in vascular development and angiogenesis.* Arterioscler Thromb Vasc Biol, 2009. **29**(5): p. 630-8.
21. Albuquerque, M.L., et al., *Shear stress enhances human endothelial cell wound closure in vitro.* Am J Physiol Heart Circ Physiol, 2000. **279**(1): p. H293-302.
22. Trappmann, B., et al., *Extracellular-matrix tethering regulates stem-cell fate.* Nat Mater, 2012. **11**(7): p. 642-9.
23. Engler, A.J., et al., *Matrix elasticity directs stem cell lineage specification.* Cell, 2006. **126**(4): p. 677-89.
24. Geiger, B., J.P. Spatz, and A.D. Bershadsky, *Environmental sensing through focal adhesions.* Nat Rev Mol Cell Biol, 2009. **10**(1): p. 21-33.
25. Wong, J., J. B. Leach, and X. Brown, *Balance of chemistry, topography, and mechanics at the cell-biomaterial interface: Issues and challenges for assessing the role of substrate mechanics on cell response*. Vol. 570. 2004. 119-133.

26. Liang, C., et al., *Biomimetic cardiovascular stents for in vivo re-endot helialization.* Biomaterials, 2016. **103**: p. 170-182.
27. Jensen, B.E., K. Edlund, and A.N. Zelikin, *Micro-structured, spontaneou sly eroding hydrogels accelerate endothelialization through presentati on of conjugated growth factors.* Biomaterials, 2015. **49**: p. 113-24.
28. Aubin, H., et al., *Directed 3D cell alignment and elongation in microe ngineered hydrogels.* Biomaterials, 2010. **31**(27): p. 6941-6951.
29. Kukumberg, M., et al., *Microlens topography combined with vascular endothelial growth factor induces endothelial differentiation of human mesenchymal stem cells into vasculogenic progenitors.* Biomaterials, 2017. **131**: p. 68-85.
30. Biela, S.A., et al., *Different sensitivity of human endothelial cells, smo oth muscle cells and fibroblasts to topography in the nano-micro ran ge.* Acta Biomater, 2009. **5**(7): p. 2460-6.
31. Lee, E.A., et al., *Extracellular matrix-immobilized nanotopographical su bstrates for enhanced myogenic differentiation.* J Biomed Mater Res B Appl Biomater, 2015. **103**(6): p. 1258-66.
32. Palmaz, J.C., A. Benson, and E.A. Sprague, *Influence of surface topogr aphy on endothelialization of intravascular metallic material.* J Vasc In terv Radiol, 1999. **10**(4): p. 439-44.
33. Rajnicek, A., S. Britland, and C. McCaig, *Contact guidance of CNS ne urites on grooved quartz: influence of groove dimensions, neuronal a ge and cell type.* J Cell Sci, 1997. **110 (Pt 23)**: p. 2905-13.
34. Wang, P.Y., et al., *Modulation of osteogenic, adipogenic and myogeni c differentiation of mesenchymal stem cells by submicron grooved to pography.* J Mater Sci Mater Med, 2012. **23**(12): p. 3015-28.
35. Suuronen, E.J., *Biomaterials for cardiac regeneration*. 2014, New York: Springer. pages cm.
36. Li, R.-K. and R.D. Weisel, *Cardiac regeneration and repair*. Woodhead Publishing series in biomaterials,. 2014, Amsterdam ; Boston: Elsevier/ Woodhead Publishing, Woodhead Publishing is an imprint of Elsevier. 2 volumes.
37. Hillberg, A.L., et al., *Improving alginate-poly-L-ornithine-alginate capsu le biocompatibility through genipin crosslinking.* J Biomed Mater Res B Appl Biomater, 2013. **101**(2): p. 258-68.
38. Park, K.M. and S. Gerecht, *Harnessing developmental processes for va*

scular engineering and regeneration. Development, 2014. **141**(14): p. 2760-9.

39. Jeon, H., et al., *Combined effects of substrate topography and stiffness on endothelial cytokine and chemokine secretion.* ACS Appl Mater Interfaces, 2015. **7**(8): p. 4525-4532.
40. Byfield, F.J., et al., *Endothelial actin and cell stiffness is modulated by substrate stiffness in 2D and 3D.* J Biomech, 2009. **42**(8): p. 1114-9.
41. N. Mason, B., J. Califano, and C. Reinhart-King, *Matrix Stiffness: A Regulator of Cellular Behavior and Tissue Formation*. 2012. 19-37.
42. Romer, L.H., K.G. Birukov, and J.G. Garcia, *Focal adhesions: paradigm for a signaling nexus.* Circ Res, 2006. **98**(5): p. 606-16.
43. Berrier, A.L. and K.M. Yamada, *Cell-matrix adhesion.* J Cell Physiol, 2007. **213**(3): p. 565-73.
44. Fujiwara, K., *Platelet endothelial cell adhesion molecule-1 and mechanotransduction in vascular endothelial cells.* J Intern Med, 2006. **259**(4): p. 373-80.
45. Mahajan, K.D., et al., *Mechanotransduction Effects on Endothelial Cell Proliferation via CD31 and VEGFR2: Implications for Immunomagnetic Separation.* Biotechnol J, 2017. **12**(9).

요약(국민초록)

자성나노입자와 그루브패턴 임베디드 하이드로젤 기반 시트제작을 통한 피부재생유도

혈관내피전구세포는 성장인자들을 포함한 생체 활성인자들을 분비, 혈관 생성 유도 능력을 가진 세포이다. 이 논문에서는 혈관내피전구세포 전달을 통해 혈관 재생을 촉진하고 상처 치유 등 손상된 곳에 혈액을 통해 산소를 포함하여 영양분을 전달하여 피부 재생을 유도하는 것을 목적으로 한다. 조직으로의 세포의 안정적인 전달을 위해서는 세포의 접착성과 세포의 보유력 및 세포의 기능을 유지하도록 하는 플랫폼의 개발이 중요하다. 이를 위해, 이 논문에서는 자성나노입자와 그루브패턴을 임베딩한 하이드로젤기반의 쉬트를 제작하였으며, 세포부착성, 세포성장, 세포증식, 및 혈관생성능력이 향상되었음을 확인하였다. 더불어 이 쉬트를 통해 피부 상처에 세포 전달을 하였을 때, 혈관생성을 유도, 가속화 된 상처치유능력을 확인할 수 있었다.

주요어: 그루브패턴, 자성나노입자, 하이드로젤, 혈관생성유도, 상처치유
학번: 2016-27768